EUROPEAN ORGANIZATION FOR NUCLEAR RESEARCH
ORGANISATION EUROPEENNE POUR LA RECHERCHE NUCLEAIRE

CERN – PS DIVISION

PS/CA/Note 99-23

CONSTRUCTION OF AN ELECTROSTATIC ANALYZER (ESA) FOR ENERGY LOSS MEASUREMENTS AT THE CERN AD

K. Knudsen[1], U. Mikkelsen[1,2], S.P. Møller[3],
R. Thompson[1] and E. Uggerhøj[3]

[1]Institute of Physics and Astronomy, Aarhus, Denmark
[2]CERN, CH-1211 Geneva 23, Switzerland
[3]Institute for Storage Ring Facilities, Aarhus, Denmark

Geneva, Switzerland
29 September 1999

Construction of an ElectroStatic Analyzer (ESA) for energy loss measurements at the CERN AD

H. Knudsen[1], U. Mikkelsen[1,2] S.P. Møller[3],
R. Thompson[1] and E. Uggerhøj[3]

[1]*Institute of Physics and Astronomy, Aarhus, Denmark*
[2]*CERN, CH-1211 Geneva 23, Switzerland*
[3]*Institute for Storage Ring Facilities, Aarhus, Denmark*

Abstract

One of the experiments to be performed under the ASACUSA collaboration at the CERN AD is a measurement of the energy loss of low energy antiprotons in thin foils and dilute gases. We describe the design of the apparatus to be used for this task including a discussion of optimization of the electrostatic optics, considering various physical constraints and measurement schemes.

Introduction

An extensive study of the energy loss of antiprotons has been performed at LEAR in the PS194 collaboration where many different solids from Z=13 to Z=79 were subject to investigations with antiprotons in the energy range 30 keV-3 MeV (although some substances were examined in a significantly smaller range of energy)[1], see figure 1. The main objective of these experiments was to determine the Barkas effect in stopping, ie. the difference in stopping power, dE/dx, between positively and negatively charged particles. For the proposed experiments, it is – as shown below – expected that the

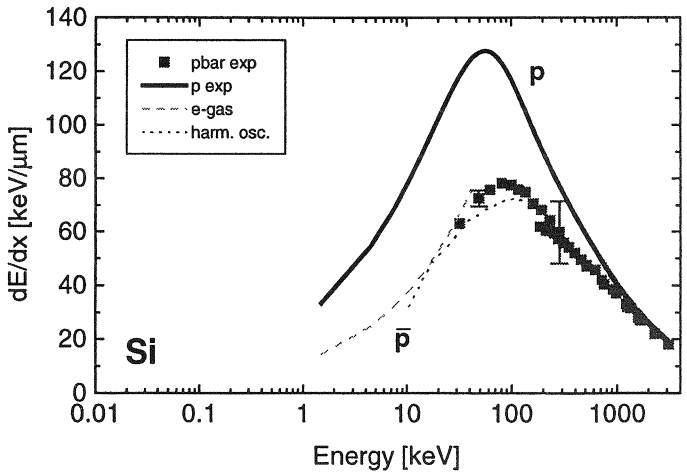

Figure 1 Stopping power for protons and antiprotons in silicon

energy-range may be extended down to about 1 keV for thin foils and possibly down to a few tens of eV for dilute gases as indicated in the figure.

At somewhat lower energies - in the range from about 20 keV and down - the proton stopping power has turned out to be surprisingly low compared to expectations[2]. To what extent this is affected by charge-exchange during the stopping process is one subject of the investigations for which we propose to construct an ESA as described below. Another subject is the onset of nuclear stopping as indicated in ref. 3 and finally one may continue the studies of the Barkas effect to examine if it remains significant well below the stopping power maximum. Figure 1 shows measured and calculated values for the stopping power of antiprotons and protons in silicon in a range of energies which is likely to be within reach for the proposed measurements.

Apparatus

The first draft for the construction of an electrostatic analyzer (ESA) to investigate the stopping power of antiprotons in thin foils and gases - as found in the first ASACUSA proposal[4] - consisted of two electrostatic deflectors between which the target was placed. The present study aims to define the necessary parameters for the actual realization of this apparatus, while at the same time providing more accurate numbers on e.g. transmission efficiency, resolution and lower limit of energy.

ESA electrodes

We choose spherical electrostatic analyzers since they provide stigmatic focusing, ie. equal focusing in the horizontal and vertical planes (for a discussion of electrostatic analyzers, see eg. ref. 5). Therefore we can obtain a small beam in both transverse directions at the position of the gas cell.

Dispersion

In order to be able to select particles of different energy and momentum, it is necessary to have a large dispersion and a focal point at the position of the gas cell. The dispersion is given as $D=2R(1-\cos(\varphi))$ for a spherical ESA, where $\Delta r=D\Delta p/p$ is the deviation from the equilibrium orbit at the output where the particle has been deflected through an angle φ. A requirement $\Delta p/p=0.05$ (The intrinsic spread of the RFQ beam is $\Delta T\equiv 9$ keV) and a minimum resolution of $\Delta r>10$ mm which with

$\Delta r=2R\cdot\Delta p/p$, $L=\varphi R$ for maximum dispersion, $\varphi=90°$, leads to $L>\Delta r\cdot\pi p/4\Delta p=$ 157 mm or $R>100$ mm.

Length of electrodes, radius of curvature

The centripetal force necessary for a curved trajectory equals $F=eE_0=mv^2/R$, where e is the magnitude of the electron charge, E_0 the electric field in the center of the gap, m the mass of the antiproton, v its speed and R the radius of curvature. The kinetic energy is $\varepsilon=\frac{1}{2}mv^2$ and the electric field for a spherical analyzer is $E(r)=E_0(r/R)^{-2}\cong E_0(1-2x/R)$ where the last approximation is for a gap d much smaller than R and $r=x+R$. . To second order in d/R this leads to the field $E_0=\Delta V/d\cdot(1-d^2/4R^2)\cong(V_1-V_2)/(r_1-r_2)$ where V_i are the potentials, r_i the radii of the analyzers and d the gap distance. Thus we get $\varepsilon=\frac{1}{4}e(V_1-V_2)\cdot(r_1+r_2)/(r_1-r_2)$ which by $R=(r_1+r_2)/2$ and $d=(r_1-r_2)$ gives $\Delta V/d=2\varepsilon/eR$. This field strength is limited due to the risk of sparks by $E_{max}=\Delta V/d|_{max}<1$ kV/mm and since $\varepsilon<\varepsilon_{max}=100$ keV we get a minimum radius of curvature $R>R_0=2\varepsilon_{max}/(eE_{max})=200$ mm. With the restriction on the electrode length $L>157$ mm we get a constraint on the deflection angle $\varphi>45°$, ie. no contradiction with the above. We choose a deflection angle of 90° (as seen above this maximizes dispersion and makes sure that the initial drift is not excessive while making place for the gas cell) and a length 392.7 mm, ie. $R=250$ mm, which leaves only a small margin against electrical break-down at the maximum energy, but surely enough margin at 50 keV. This radius of curvature coincides with that supplied for standard beam line tubes and will thus secure minimum cost.

Gap distance

Simulations show that the maximum beam radius (2σ, 95% of all particles) in the ESA is of the order 9 mm which means that half the gap distance must exceed this with some safety margin to account for mis-steered beam etc. (still, 68% is contained within 4.5 mm) Therefore we choose $d=20$ mm and get $\Delta V_{max}=d\cdot E_{max}=2\varepsilon_{max}d/eR$ to be $\Delta V_{max}[\text{kV}]=d[\text{mm}]/1.25$ which means maximum 8 kV on each electrode.

The gap distance is also limited by $d\ll L$ and $d\ll h$ where h is the height of the electrodes to avoid significant edge focusing effects. Thus the choice of d sets a limit on h to be at least 50 mm. At the same time, the electrodes should fit into a standard beam tube with an inner diameter of 150 mm with a spacing of at least 20 mm to each side. With

these restrictions, we choose h to be 60 mm to make room for the mounting and screening plates to make the field as homogenous as possible between the ESAs.

Gas cell

First, the beam size must not vary excessively within the volume. This variation is given (assuming a focus at the center) as $r_e/r_c \cong (1+s^2/\beta^2)^{1/2}$ where r_e/r_c is the ratio of beam radii at the center and the edge of the gas cell a distance s away. $\beta \cong 5$ cm is the Twiss parameter which determines the beam size from $(\varepsilon_e \beta)^{1/2}$ where $\varepsilon_e \cong 100$ mm·mrad is the emittance. From $s=L_g/2$, the calculated value $r_c \cong 1$ mm (again 95% of all particles) and the constraint $r_e < 1.5$ mm given by the diameter of the entry- and exit-windows, we get $L_g < 2\beta((r_e/r_c)^2-1)^{1/2} = 112$ mm.

The length of the gas cell must also be chosen such that energy loss in a gas of reasonable pressure is comparable to the loss in the two windows confining the gas. Windows for the gas cell can be made of aluminum or carbon, Ø 3mm, Δx=500 Å thick. The energy loss is essentially proportional to the density of electrons[6]: $-dE/dx \propto NZ$ and since the pressure $p=nR_gT/V$ and the atomic density in Å^{-3}, $N=n/V=0.6022 \cdot \rho/M$, with M the atomic mass in u and the density ρ in g/cm^3 we get with the gas constant R_g=8.314 J/(mol·K) $N_0=2.45 \cdot 10^{-5}$ atoms/Å^{-3} at p=1 atm. To limit the extent of gases we set Z>5 and a reasonable pressure p=1/100 atm. (The number of collisions is $n_{coll}=N\sigma\Delta x$ where $\sigma \cong 1$ Å^2 is the excitation cross section, so the pressure must be $p \gg 1$ atm./$(N_0\sigma\Delta x) > 3.6 \cdot 10^{-5}$ atm. to fulfill $n_{coll} \gg 1$ for the stopping power measurement to make sense). This leads to a restriction on the gas cell length of $L_g > 2\Delta x (NZ)_{Al}/(NZ)_{gas} = 3.2 \cdot 10^6 \cdot 1000$ Å/Z=64 mm. We choose L_g = 100 mm.

Length of drifts

Clearly, the drift between the ESAs must exceed L_g and leave room for diagnostics and apertures. Once the length of this drift region is fixed, the initial and final drifts are found from $L_a=L_c= 2R^2/L_b$ (with φ=90°) which ensures a focus in the center of the gas cell. One must therefore find a compromise between a small $L_a=L_c$ or a small L_b. To get a fairly small beam size through the ESAs we choose $L_a=L_c$=250 mm and L_b=500 mm.

Simulations

Two kinds of simulations were performed. A simulation by use of SIMION was done to study influence of edge effects, apertures and other realistic parameters, see figure 5. For instance, it turns out that the position of the vertical focus at the gas cell is influenced by the height of the electrodes, *h*.

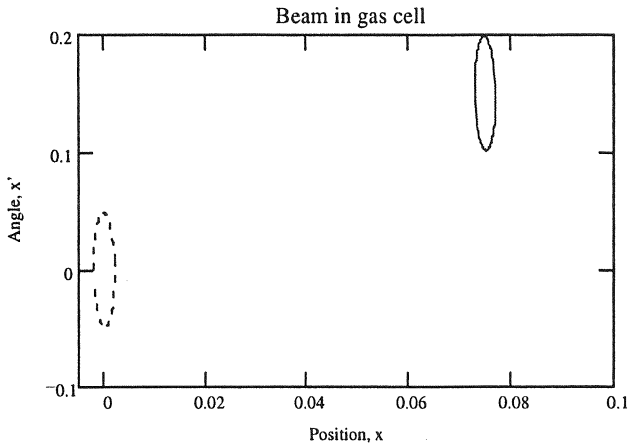

Figure 2 Phase-space of the beam at the position of the gas cell. The full-drawn ellipse represents the beam including dispersion and the dashed excludes dispersion. The values used are an energy of 60 keV and a spread of 9 keV.

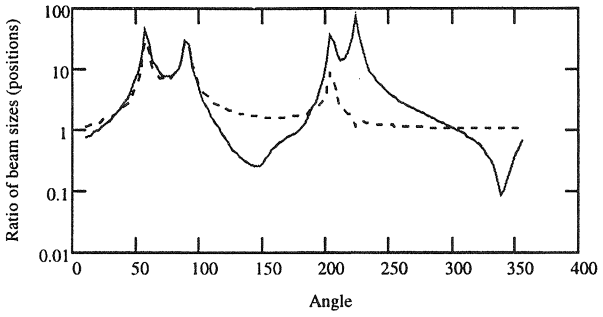

Figure 3 Ratio of beam size+position with and without dispersion as a function of angle for L=0.3927 m. The dashed curve is the effect of dispersion through the last ESA only, whereas the full drawn shows the effect with dispersion in both ESAs.

The second calculation was done by use of MathCad to study the behaviour of beam size, dispersion, divergence and stability as a function of the ESA angle, φ, the drift lengths, L_a, L_b, L_c and the electrode length, L. Transformation of the initial Twiss parameters was done by matrix multiplication through the entire electrostatic lattice. Consistency with the behaviour predicted by SIMION was confirmed and the free variables were optimized to yield a large effect of dispersion at the output and in the gas cell while keeping the beam size small in both locations. At the same time, the stability of the solutions against errors of construction, eg. angle or electrode length errors could be checked, see appendix A. The figures 2-5 show some examples.

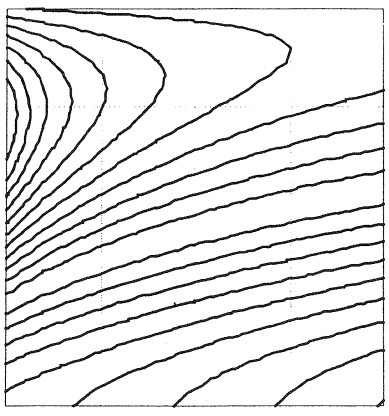

mtrx_sfz_mid_y

Figure 4 Horizontal and vertical beam size at the gas cell as a function of angle (y-axis, from 0 to 180 degrees) and length of electrodes (x-axis, from 10 to 50 cm). The colours show the size ranging from 0.5 cm (darkest) to 5.5 cm (lightest) in steps of 0.5 cm.

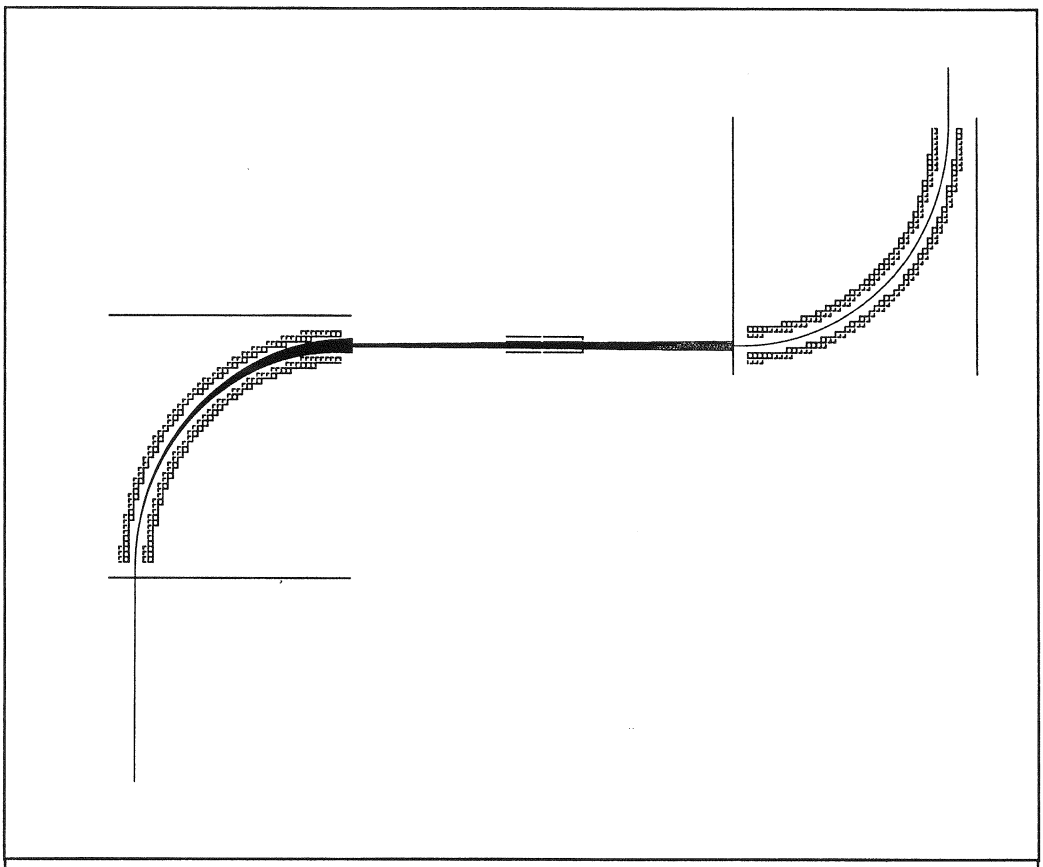

Figure 5 SIMION simulation of the trajectory through the setup for different energies. The selections imposed by the apertures at the entry and exit of the ESAs are clearly seen.

Beam steering

Parallel plate deflectors can be inserted upstream the first ESA and up/downstream the gas cell to correct for wrong steering. The deflection angle, α, of a particle with energy ε through a parallel plate deflector of length, L_p, with a field $\Delta V_p/d_p$ is given as $\alpha \cong e\Delta V_p L_p/2\varepsilon d_p$. Thus, even for the 100 keV beam a short assembly, say $L_p = d_p = 20$ mm, would suffice.

For additional focusing, an Einzel lens could be inserted on the entry side of the ESAs. The focal length, f, of an Einzel lens consisting of 3 cylindrical electrodes of diameter D and length $0.9D$ separated by $0.1D$ is given as $f=0.91 \cdot D\varepsilon/V$ where V is the potential of the outer electrodes with respect to the central one which is kept at ground[7]. Thus, a lens with D=2 cm would yield a minimum focal length of 18 cm at 10 keV with the maximum voltage, V=2 kV.

As it turns out, in order to make a compact apparatus, the gas cell can not be positioned exactly in the center between the two outer spherical deflectors. The einzel lens is thus essential to move the focal point of the beam such that the counting rate can be maximized.

PARAMETER	NAME	VALUE	CONSTRAINTS
ε	Beam energy	0-120 keV	Given by RFQ
d	Gap distance	20 mm	Max. beam diameter = 18 mm
h	Electrode height	60 mm	$d \ll h$, $h<150$ mm
ΔV	Potential diff.	0-16 kV	$\Delta V/d=2\varepsilon/eR$
R	Curvature radius	250 mm	$R>R_0=2\varepsilon_{max}/(eE_{max})=200$ mm
L_a	Final drift	250 mm	$L_c=2R^2/L_b$, $\varphi=90°$
L_b	Space between ESAs	500 mm	$L_b> 2d_j+L_g$
L_c	Initial drift	500 mm	$L_c=2R^2/L_b$, $\varphi=90°$
d_j	distance ESA - aperture	15 mm	$d_j>\Delta V/2$kV·1mm
φ	ESA angle	90°	$\varphi=L/R$, max. dispersion
L	ESA length	392.7 mm	$L>\Delta r\cdot\pi p/4\Delta p=157$ mm
L_g	Gas cell length	100 mm	$L_g<2\beta((r_e/r_c)^2-1)^{1/2}=112$ mm $L_g>2\Delta x(NZ)_{Al}/(NZ)_{gas}=64$ mm

Table 1 Choice of parameters for the construction of the ESA

Particle detection and diagnostics

To be able to get the beam through the whole setup, we need diagnostics along the way. We choose a retractable phosphorized channelplate screen with a camera in front of the gas cell and at the exit of the last ESA.

Furthermore, as the number of particles which will appear at the end detector is quite small for the low energy measurements, particle counting can be enabled by conversion of the analog signal in an ADC while the beam spot is visible by use of a camera.

Estimated countrates, lower limit of energy

The lower limit of energy at which it makes sense to derive a stopping power is essentially determined by the energy loss straggling in the Al (or C) windows. Taking a total of Δx=1000 Å for the windows we get from Bohr's formula[8], $\Omega^2=4\pi NZ_2e^4\Delta x$ a straggling of Ω_{Al}=1.4 keV and Ω_C=1.3 keV (the so-called LS modification to the straggling formula[9] would lead to only Ω_{Al}=0.4 keV and Ω_C=0.4 keV) at 4 keV. The energy loss in Al from an electron gas calculation[10] which includes the Barkas effect (see eg. ref. 1), $\Delta E=0.9C_1\cdot 4Z_1ve^2\Delta x/(3\pi\alpha ca_0^2)$ equals 2.4 keV with C_1=0.31 for Al and about the same for C, also for antiprotons at 4 keV.

Furthermore, the increase of the emittance following the scattering in the foil is given as $\Delta\varepsilon=\pi\beta\theta^2/2$ where θ is the RMS angle from multiple scattering found from $\theta=\pi aN\Delta x Z_1 Z_2 e^2/(Mv^2)$ and $a=0.8853a_0 Z_2^{-1/3}$ is the Thomas-Fermi screening distance[11]. This will enlarge the beam at the output such that starting with 10^7 particles and accounting for RFQ deceleration efficiency, emittance increase, straggling and apertures we get around 50 particles through the whole setup into a detector of 10 mm width. This detector width yields an energy resolution of 0.3 keV and the 3 mm aperture at the gas cell selects the initial beam to a width of 0.4 keV. It thus seems reasonable to state that around 4 keV is the lower limit for a measurement of the energy loss (the gas in the gas cell has not even been taken into account) for the proposed setup. However, with a few mm aperture at the output, it should be possible also to measure the energy straggling down to an energy of 4 keV - this may be of interest for protons as well as for antiprotons.

In the case of a continuation of the measurement by the use of foils, the constraint $\Delta E/E<1$ calls for thin targets, $E>2.9C_1^2Z_1^2\Delta x^2e^4/(M\pi^2\alpha^2c^2a_0^4)=1.5\cdot10^{-3}\cdot\Delta x^2$ eV/Å^2 for Al. This may be necessary since the stopping power in foils may not be described in the same way as that of gases at low energy even though calculations indicate that the dependence of the stopping power per target electron on the density of electrons is very weak over several orders of magnitude[12]. Foils of 500 Å Si, Al or C can be

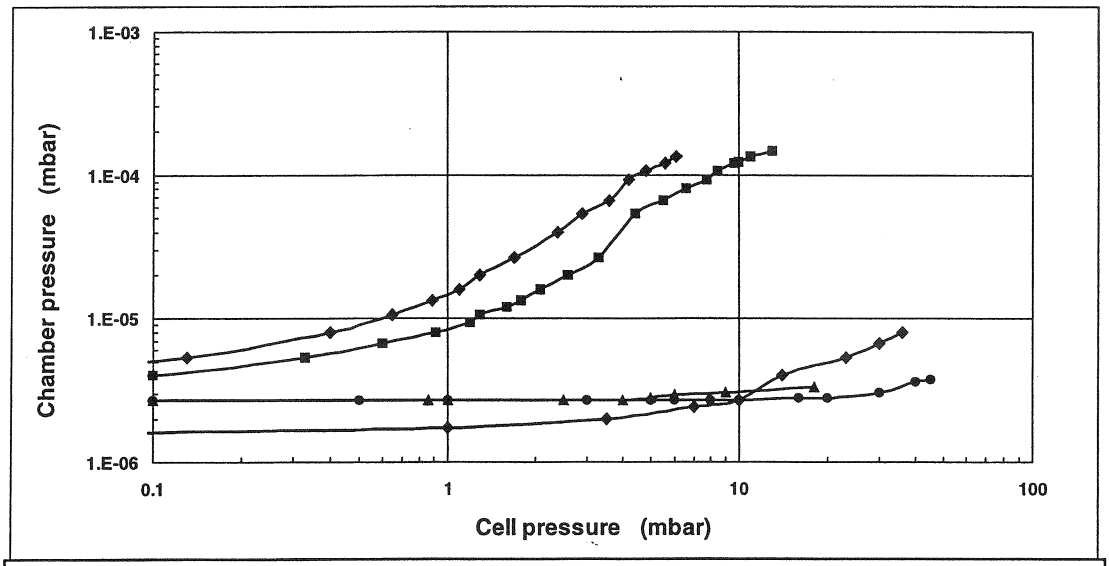

Figure 6 Chamber pressure as a function of pressure in the gas cell. The endpoint of each curve indicates the pressure at which the window ruptures.

prepared where the energy loss amounts to about 0.5 keV which would bring the realistic minimum of energies down to a few keV. Such foils with a diameter of 3 mm

have recently been tested and shown to withstand a pressure of up to about 40 mbar, see figure 6. From this figure it is also seen that not all foils are of the same quality in terms of homogeneity.

One way to get to even lower energies is by using a differentially pumped gas cell, ie. simply the same setup except for the entry- and exit-windows. One can then calibrate the average pressure in the open gas cell by measuring stopping powers in a region overlapping in energy with those of the complete gas cell. This may bring the lower limit of energies down to the eV region to verify earlier indirect evidence of the nuclear stopping power[3]. The conductivity of a Ø 3 mm cylinder of length 10 mm sufficiently low and furthermore two discs with Ø 10 mm holes are introduced to isolate the region of the gas cell to the turbo pump. Since the vacuum requirements for the RFQ is 10^{-6} or better, a turbopump is needed at the gas cell[13] as well as a pump supplied by CERN at the exit of the RFQ.

Calibration - cross check

We propose to calibrate the setup in terms of energy by a measurement of the time-of-flight of the ions. This can be done with respect to the RF cycle of the RFQ and the AD and by measuring the arrival time for the undecelerated 5.31 MeV antiproton beam from the RFQ. For this reason, and to dispose of the undecelerated beam without generating too many pions that can trigger downstream detectors, a hole in the first spherical analyzer covered with a fine mesh will be made. The dump will be constructed from a 2 mm thick tantalum foil placed at the end of a steel cylinder. This has the advantage that the main component of induced activity (which may be significant after tests with protons) is low energy electrons which will not penetrate the steel.

As an alternative to the undecelerated antiprotons, one may use a source of electrons with energy similar to that obtained for the antiprotons from the RFQ.

In terms of pressure in the gas cell a precise measurement should not be too difficult e.g. by means of a baratron, since it is a confined volume where tests of the windows show very limited leakage through the windows for pressures in the range up to 1/100 atm.

Measurement scheme

Assuming an efficiency for the extraction from the AD combined with that of the RFQ to be 50% with one extraction per minute, we get 720 shots per day. We propose to measure at (1, 2,) 5, 10, 20, 50, 80 and 100 keV, each measured point consisting of a 'scan' around the most probable energy loss, if possible to determine the energy straggling. Each 'scan' consisting of 10 points it can be expected to finish one foil or gas in a couple of hours. Thus, three-four days of dedicated running would be enough for the measurement (under these somewhat optimistic assumptions), excluding time for the setup and initialisation. Table 2 shows the precision and count rates that can be expected from a 500 Å aluminium foil.

E [keV]	ΔE [keV]	τ [10^{-7}]	δ [keV/cm]	Ω [keV]	θ [mrad]	$\Delta\varepsilon$ [π mm·mrad]
1	0.61	50	0.10	0.20	2076	107700
2	0.86	100	0.17	0.23	1038	26960
5	1.4	250	0.31	0.29	415	4312
10	1.9	490	0.45	0.35	208	1078
20	2.7	880	0.66	0.42	104	269
50	4.3	1400	1.1	0.52	42	43
80	5.5	1590	1.4	0.59	26	17
100	6.1	1630	1.5	0.62	21	11

Table 2 Selected antiproton energies and their energy loss[9], simulated transmission, output sensitivity, energy straggling[8], multiple Coulomb scattering[10] and emittance increase (β=5 cm) for a 0.05 mm Al foil.

Appendix

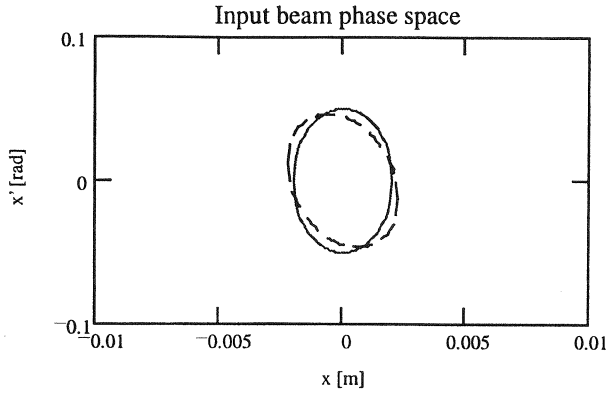

Figure 7 Horizontal and vertical phase-space.

Figure 7 shows the input beam phase space as used for the calculations of beam sizes and divergences through the setup. The full-drawn line is the horizontal phase-space and the dashed line represents the vertical phase-space of the decelerated particles (nominal 60 keV) after the RFQ.

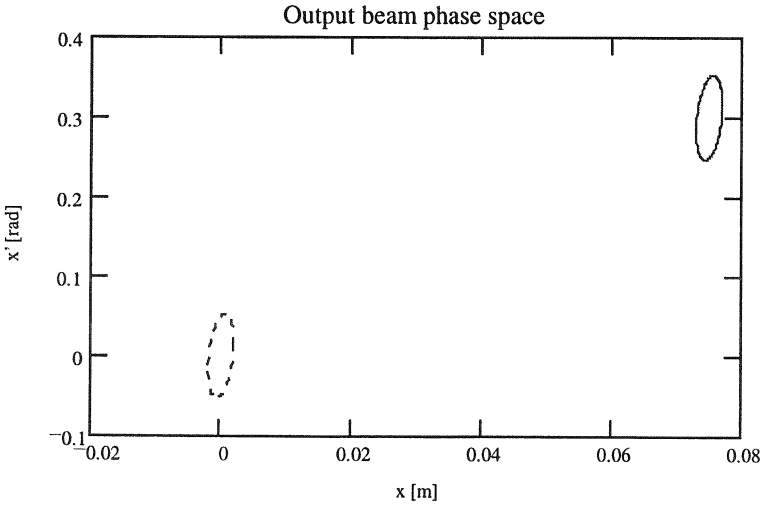

Figure 8 Phase-space of the beam at the position of the final detector

In figure 8 the full-drawn line is the horizontal phase-space for a 69 keV antiproton beam (nominal beam with energy spread and ESA dispersion included) after the last ESA and the dashed line represents the nominal 60 keV beam. Clearly, a small (few mm) aperture will select a fraction of particles with a relatively well-defined energy. Also, the parameters used give a focal point at the final detector as seen from the orientation of the ellipse – this ensures a minimal ambiguity between emittance and energy spread.

Figure 9 shows the beam size and divergence after the two ESAs and the final drift as a function of electrode length of the two ESAs where the deflection angle is fixed to 90 degrees. The width of the minimum around L=0.25 m/90°=π/8 m is sufficiently wide that there should be no problems connected to edge-effects (integrated field length) or mechanical tolerances.

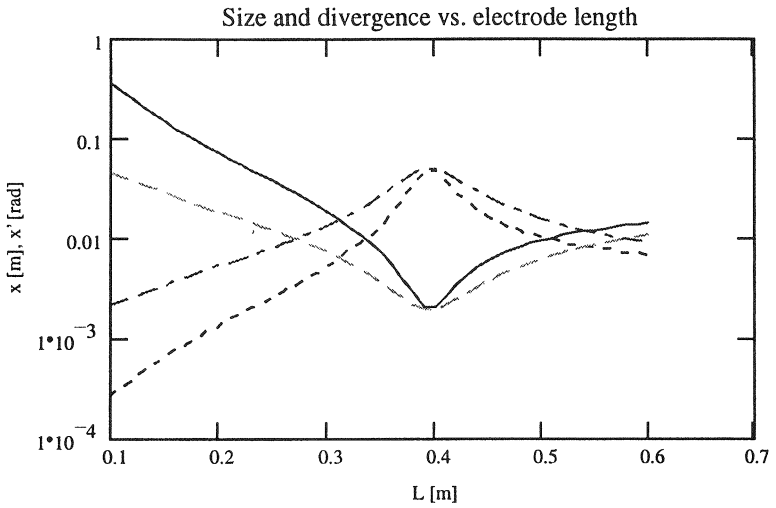

Figure 9 Beam size and divergence as a function of electrode length for fixed deflection angle. The full-drawn and dotted lines represent the size and divergence at the end of the setup, the dashed and dash-dotted represent the size and divergence at the gas cell.

Figure 10 shows the dependence of beam size and divergence on the deflection angle. From this it is seen that although there is a deeper minimum corresponding to the size at the end for an angle of each ESA around 130°, it is rather narrow and does not coincide with a minimum at the gas cell.

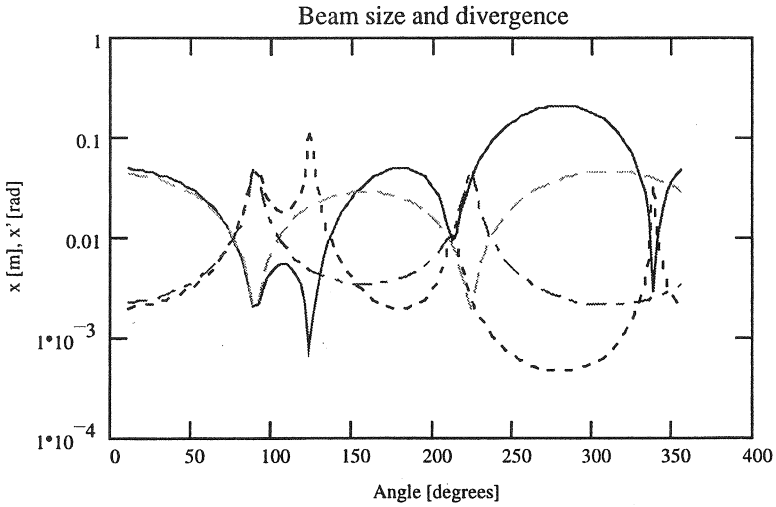

Figure 10 Beam size and divergence as a function of electrode deflection angle for fixed length. The full-drawn and dotted lines represent the size and divergence at the end of the setup, the dashed and dash-dotted represent the size and divergence at the gas cell.

Figures 11-13 show 3-D construction drawings[14] of the entire setup where the electrostatic deflectors, the gas cell and its apertures, the beam dump, the HV-feedthroughs and the mountings are clearly seen.

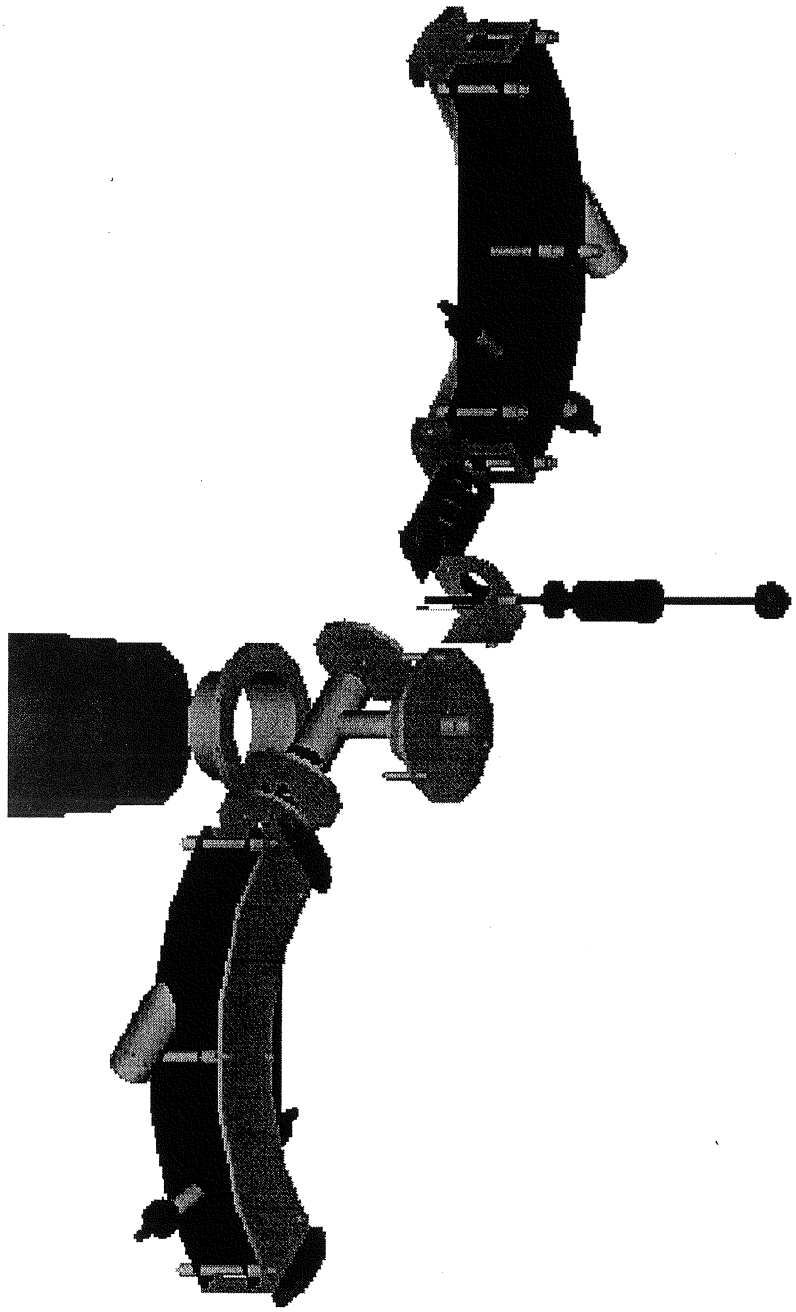

Figure 11-12 Views of the ESA apparatus

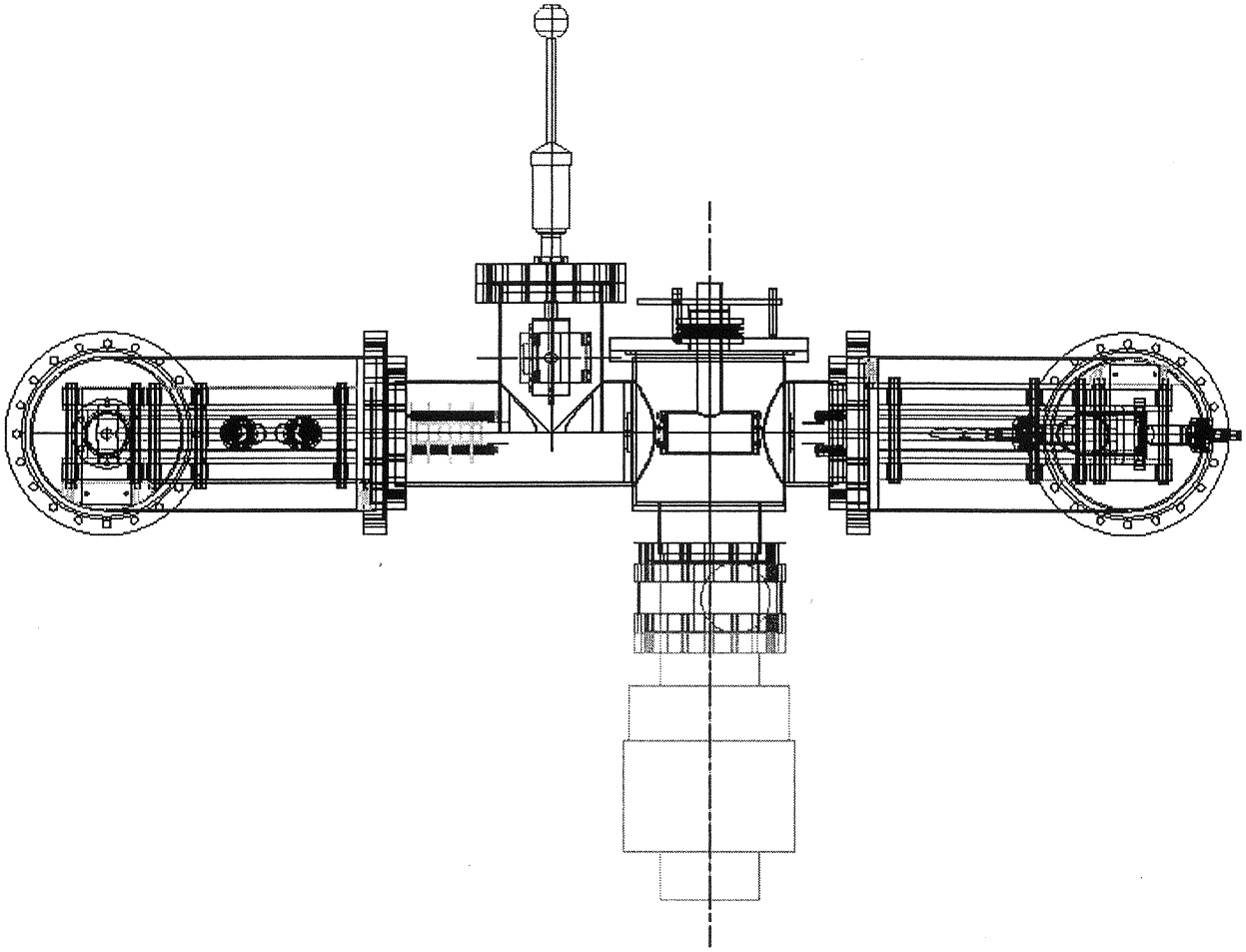

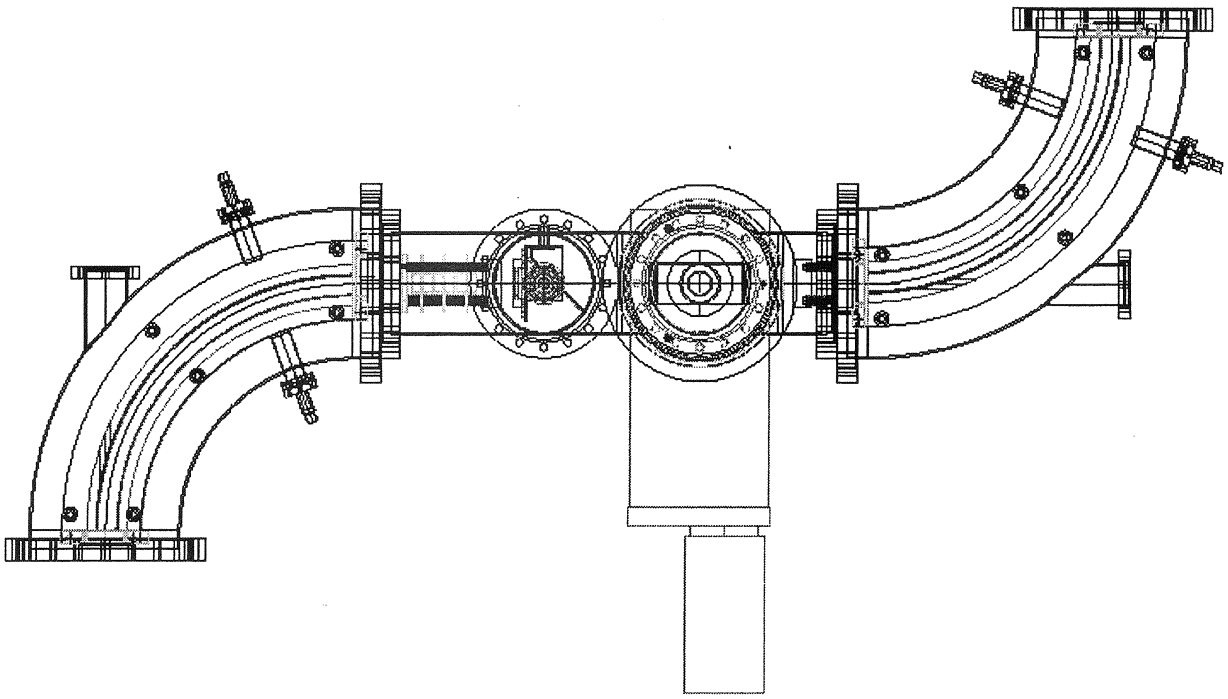

References

[1] S.P. Møller *et al.*, Phys. Rev. A **56**, 2930 (1997)
[2] R. Golser and D. Semrad, Phys. Rev. Lett. **66**, 1831 (1991); R. Golser and D. Semrad, Nucl. Instr. Meth. B **69**, 18 (1992)
[3] M. Agnello *et al.*, Phys. Rev. Lett. **74**, 371 (1995)
[4] T. Azuma *et al.* (ASACUSA Collaboration), CERN/SPSC 97-19, CERN/SPSC P-307
[5] P. Dahl - Introduction to electron and ion optics, Academic Press, 1973
[6] H.A. Bethe, Ann. Phys. **5**, 325 (1930)
[7] E. Harting and F.H.Read - Electrostatic lenses, Elsevier Scientific 1976
[8] N. Bohr, Phil. Mag. (6) **30**, 581 (1915)
[9] J. Lindhard and M. Scharff, Kgl. Dan. Vid. Selsk. Mat. Fys. Medd. **27**, No. 15 (1953)
[10] A.H. Sørensen, Nucl. Instr. Meth. B **48**, 10 (1990)
[11] P. Sigmund and K.B. Winterbon, Nucl. Instr. Meth. **119**, 541 (1974)
[12] A. Belkacem and P. Sigmund, Nucl. Instr. Meth. B **48**, 29 (1990)
[13] H. Klette, CERN, private communication

[14] We wish to thank K. Iversen, ISA, Aarhus, for producing the construction drawings and for making everything fit